

Weakly invasive metrology: quantum advantage and physical implementations

M. Perarnau-Llobet,^{1,2,3} D. Malz,^{1,2} and J. I. Cirac^{1,2}

¹*Max-Planck-Institut für Quantenoptik, D-85748 Garching, Germany.*

²*Munich Center for Quantum Science and Technology (MCQST), Schellingstrasse 4, D-80799 München*

³*Département de Physique Appliquée, Université de Genève, Genève, Switzerland*

(Dated: June 8, 2022)

We consider the estimation of a Hamiltonian parameter of a set of highly photosensitive samples, which are damaged after a few photons N_{abs} are absorbed. The samples are modelled as a two mode photonic system, where photons simultaneously acquire information on the unknown parameter and are absorbed at a fixed rate. We show that arbitrarily intense coherent states can obtain information at a rate that scales at most linearly with N_{abs} , whereas quantum states with finite intensity can overcome this bound. The quantum advantage scales like N/N_{abs} (where N is the number of photons in the quantum state), so that few-photon entangled states can already surpass the classical bound when N_{abs} is small. We discuss an implementation in cavity QED, where Fock states are both prepared and measured by coupling atomic ensembles to the cavities.

INTRODUCTION

One exciting prospect of quantum technologies are more precise photonic measurements through the use of quantum correlations [1–5]. Given a fixed (average) photon number N , a variety of quantum states surpasses the shot-noise limit imposed by coherent states, notably squeezed, NOON or twin Fock states [6–8]. One of the motivations to limit N is that some photosensitive materials, such as biological samples [9–14], may be damaged when they absorb too many photons. However, in this case it may be more meaningful to constrain the number of photons absorbed by the sample N_{abs} , instead of N [12, 15]. While in interferometric measurements this constraint is equivalent to fixing the total number of photons, we will show here it leads to qualitatively new results in frequency measurements in which photons are allowed to interact continuously with the sample.

In frequency measurements, both the probe size (e.g. the number of photons N) and the total time T are resources for quantum metrology [8, 16–18], and interesting interplays between both appear when the probe is subject to noise or decoherence [16–23]. Optimal metrological protocols for a fixed N and T have been considered for atomic measurements [16–23], non-linear photonic systems [24], many-body open quantum systems [25], and time-dependent Hamiltonians [26–28]. Such time-optimized protocols can lead to a supraclassical scaling with N of the measurement precision for specific types of correlated or directional noise [19–23, 29–32], and to a constant advantage for uncorrelated noise [16, 33–36].

Here, we shall not put the constraint on N , but on the energy that the sample can absorb (N_{abs}). This subtle difference turns out to have important consequences: quantum metrological protocols involving a small amount $N \approx 5 - 10$ of photons and a finite amount of samples, can overcome classical strategies using coherent states of (potentially) arbitrary intensity and an arbitrarily large number of samples. We also discuss robustness to imperfections (non-ideal detectors, finite preparation and measurement times), and show that such enhancements can be realized in

state-of-the-art technologies using a cavity or circuit QED set-up [37, 38].

FRAMEWORK AND PHYSICAL SETUP

We model the “delicate sample” as a two-mode photonic system, $H = H_0 + gH_{\text{int}}$ with $H_0 = \omega(a^\dagger a + b^\dagger b)$ and $H_{\text{int}} = (a^\dagger b + ab^\dagger)/2$. We wish to estimate the interaction strength g between modes (g has units of frequency and we set $\hbar = 1$). The inference process is mediated by photons, which can also be absorbed by the sample leading to its degradation. The latter process is modelled as a Markovian dissipative process, so that the time evolution of the photonic state ρ reads:

$$\dot{\rho} = -i[H_0 + gH_{\text{int}}, \rho] + \gamma(\mathcal{D}_a(\rho) + \mathcal{D}_b(\rho)) \quad (1)$$

with $\mathcal{D}_x(A) = xAx^\dagger - \frac{1}{2}\{x^\dagger x, A\}$. With time, information on g is encoded in ρ , but also photons are lost (absorbed). These two dynamical processes decouple, so that the evolution can be described as two independent channels: $\rho(t) = C_{g,t}^{\text{uni}} \circ C_{\gamma,t}^{\text{diss}}[\rho_0]$, with $C_{\gamma,t}^{\text{diss}}[\rho] = e^{-\gamma t(\mathcal{D}_a + \mathcal{D}_b)}[\rho]$ and $C_{g,t}^{\text{uni}}[\rho] = e^{-i(H_0 + gH_{\text{int}})t} \rho e^{i(H_0 + gH_{\text{int}})t}$.

If the initial state ρ_0 contains N photons, the (average) number of absorbed photons is given by

$$N_{\text{abs}}(t) = \text{Tr}[\rho(t)\hat{N}] = N(1 - e^{-\gamma t}), \quad (2)$$

where $\hat{N} = a^\dagger a + b^\dagger b$ counts the total number of photons. We shall assume that the delicate sample is destroyed when $N_{\text{abs}}(t) = N_{\text{abs}}$, which sets a maximum available time for information acquisition. This constrains the possible estimation schemes and, to some extent, N_{abs} can be seen as a resource: a larger N_{abs} enables us to obtain more information (and/or in a faster manner) from a single sample.

In order to estimate g , we consider the following scenario: We have at our disposal a large number of delicate samples that we can measure sequentially for a total time T . The same estimation scheme, or test, is applied to each sample. In each test, a photonic state ρ_0 is prepared, it evolves for some time t according to (1) reaching ρ_g , and is measured by an observable Π ,

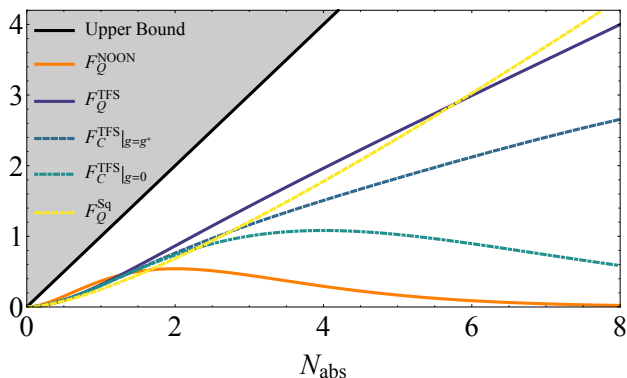


Figure 1. \mathcal{F}_Q for TFS and NOON states (Eqs. (8) and (10)), and \mathcal{F}_C for TFS at $g = 0$ and $g = g^*$ using photon number resolved measurements, \mathcal{F}_C for optimised two mode squeezed states with homodyne measurements (details in the Appendix). All quantities are computed in the Poisson limit ($N \rightarrow \infty$, $t \rightarrow 0$), so that only states with Heisenberg scaling can yield non-zero information in this plot. Parameters: $\gamma = 1$.

which yields the outcome s_j with probability p_j . The whole experiment consists of ν tests, with each test taking a time $t = T/\nu$, which must satisfy $N_{\text{abs}}(t) \leq N_{\text{abs}}$. When $\nu \gg 1$ (the regime of interest in this paper), the uncertainty $\Delta^2 g$ of an unbiased estimator of g satisfies [39–41]:

$$\Delta^2 g \geq \frac{1}{\nu \mathcal{F}_C} \geq \frac{1}{\nu \mathcal{F}_Q}. \quad (3)$$

Here, $\mathcal{F}_C = \sum_j p_j^{-1} (\partial p_j / \partial g)^2$ is the Classical Fisher Information (CFI) and \mathcal{F}_Q is the quantum Fisher Information (QFI), which will be defined later for each case of interest, and characterizes the potential of ρ_g for estimating g with an optimal measurement [41]. Our goal is to minimize (3) for both coherent and quantum (e.g. Fock, NOON, or squeezed) states, and to find the corresponding optimal strategies.

It is worth pointing out that, defining $a_{\pm} \equiv (a \pm b^\dagger)/\sqrt{2}$, we can rewrite H as $H = (\omega + g)a_+^\dagger a_+ + (\omega - g)a_-^\dagger a_-$, so an alternative interpretation of this framework is that we are estimating the frequency difference between two modes. In terms of the original modes a and b , both pictures are physically equivalent if a balanced beamsplitter is applied to the input (and output) light. With this transformation, it is also clear that the problem at hand can be formally mapped to standard Mach-Zehnder interferometry with $\varphi = gt$, where photon absorption corresponds to a symmetric (time-dependent) photon loss. This map naturally enables us to use techniques and results developed in this context [1–3].

Optimal classical strategy. Let us first analyze the optimal strategy using coherent states. We consider as an input state $\rho_0 = |g_0\rangle\langle g_0|$ with $|g_0\rangle = |\cos(\theta)\sqrt{N}, \sin(\theta)\sqrt{N}\rangle$. The dissipative channel acts upon the initial state as $|\phi\rangle = \mathcal{C}_{\gamma,t}^{\text{diss}}[g_0] = |\cos(\theta)\sqrt{e^{-\gamma t}N}, \sin(\theta)\sqrt{e^{-\gamma t}N}\rangle$. Since the state remains pure, we can quantify the QFI of $\rho_g =$

$\mathcal{C}_{g,t}^{\text{uni}}[|\phi\rangle\langle\phi|]$ as $\mathcal{F}_Q = 4t^2(\langle\phi|H_{\text{int}}^2|\phi\rangle - (\langle\phi|H_{\text{int}}|\phi\rangle)^2)$ [41], obtaining:

$$\mathcal{F}_Q^{\text{coh}} = t^2 N e^{-\gamma t}, \quad (4)$$

which is the shot-noise-limit. Using $N_{\text{abs}} = N(1 - e^{-\gamma t})$ and $t = T/\nu$, the accumulated QFI in a time T reads: $\nu \mathcal{F}_Q^{\text{coh}} = T^2 N_{\text{abs}} e^{-\gamma T/\nu} / (1 - e^{-\gamma T/\nu}) \nu$. This expression increases monotonically with ν , so its maximum $(\Delta g)_{\text{coh}}^{-2} \equiv \max_{\nu}(\nu \mathcal{F}_Q^{\text{coh}})$ is obtained for $\nu \rightarrow \infty$:

$$(\Delta g)_{\text{coh}}^{-2} = \frac{T}{\gamma} N_{\text{abs}}. \quad (5)$$

Strictly speaking, this bound can be saturated by testing $\nu \rightarrow \infty$ samples, each for an infinitesimally small time $t \rightarrow 0$ using a number $N \rightarrow \infty$ of photons, in such a way that both $N_{\text{abs}} = \gamma t N$ and $T = \nu t$ remain constant. We call this theoretical limit ($N, \nu \rightarrow \infty$ and $t \rightarrow 0$, with both $N_{\text{abs}} = \gamma t N$ and $T = \nu t$ fixed) the *Poisson limit*, which will play a relevant role in this work.

QUANTUM STRATEGIES

We now move to quantum resources. We begin by deriving an upper bound on \mathcal{F}_Q given arbitrary quantum states. We use the results of Refs [33–35, 42, 43], where the upper bound $\mathcal{F}_Q \leq N(1 - \mu)/\mu$ is obtained for an optical interferometer with symmetric photon loss in both arms, as quantified by μ (the probability of photon loss in each arm of the interferometer). In the context studied here, this translates as: $\mathcal{F}_Q \leq t^2 N(1 - \mu)/\mu$ with $\mu = 1 - e^{-\gamma t}$ and $N_{\text{abs}} = \mu N$. Taking the Poisson limit ($t \rightarrow 0$, $N \rightarrow \infty$ and N_{abs} constant) yields

$$\mathcal{F}_Q \leq \frac{N_{\text{abs}}}{\gamma^2}. \quad (6)$$

Hence, in principle a finite amount of information can be obtained from a single measurement as $t \rightarrow 0$, which implies $(\Delta g)^2 = (\nu \mathcal{F}_Q)^{-1} \rightarrow 0$ for any $T, N_{\text{abs}} > 0$, i.e., an arbitrarily large advantage over the classical bound (5). Intuitively, this can be understood by noting that $\mathcal{F}_Q \sim t^2 N^2$ for states featuring Heisenberg scaling, which remains constant in the Poisson limit. We now calculate \mathcal{F}_Q for relevant quantum states in this limit, and discuss the attainability of (6).

We start by the paradigmatic case of twin-Fock states (TFS) [7, 44, 45]. To compute $\mathcal{F}_Q^{\text{TFS}}$, we note that given $\rho_g = \sum_s q_s |\phi_s(t)\rangle\langle\phi_s(t)|$, with $|\phi_s(t)\rangle = e^{-itgH_{\text{int}}} |\phi_s\rangle$ and $\langle\phi_s|\phi_l\rangle = \delta_{sl}$; the QFI reads

$$\mathcal{F}_Q^{\text{TFS}} = 4t^2 \left[\sum_i q_i (\Delta H_i)^2 - \sum_{i \neq j} 2q_i q_j |H_{ij}|^2 (q_i + q_j)^{-1} \right], \quad (7)$$

with $(\Delta H_i)^2 = \langle\phi_i|H_{\text{int}}^2|\phi_i\rangle - (\langle\phi_i|H_{\text{int}}|\phi_i\rangle)^2$ and $|H_{ij}|^2 = |\langle\phi_i|H_{\text{int}}|\phi_j\rangle|^2$ [41, 46]. In our case, the initial state is $\rho_0 = |\phi_0\rangle\langle\phi_0|$ with $|\phi_0\rangle =$

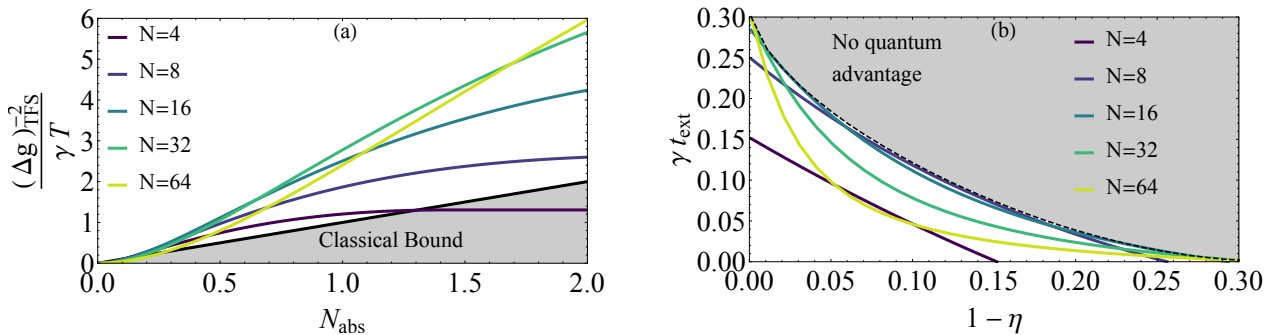


Figure 2. (a) $(\Delta g)_{\text{TFS}}^2/\gamma T$ as a function of N_{abs} for TFS of different N with $\eta = 0.96$ and $\gamma t_{\text{ext}} = 0.04$, together with the classical bound (5). The numerical results for TFS are obtained by computing $\max_{\nu}(\nu \mathcal{F}_Q^{\text{TFS}})$ (using the exact expression (7)) given the constraints $t\nu = T$ and $N_{\text{abs}}(t) \leq N_{\text{abs}}$ with $N_{\text{abs}}(t)$ in (2). The optimal ν is well approximated by $\nu/T\gamma \approx N/N_{\text{abs}}$. (b) In grey, region where quantum advantages are not possible with TFS of any N and with $N_{\text{abs}} = 1$. The curves are implicitly defined by $(\Delta g)_{\text{TFS}}^2/(\Delta g)_{\text{coh}}^2 = 1$ given TFS of different photon number.

$|n, n\rangle$ and $N = 2n$, and evolves in time as: $\rho_g = \sum_{k,j} p_k p_j |\phi_{k,j}(t)\rangle \langle \phi_{k,j}(t)|$ with $|\phi_{k,j}\rangle = e^{-itgH_{\text{int}}} |n-k, n-j\rangle$, $p_k = \binom{n}{k} \mu^k (1-\mu)^{n-k}$ and $\mu = 1 - e^{-\gamma t}$. Plugging these into \mathcal{F}_Q , and taking the Poisson limit ($t \rightarrow 0$ with $2n\gamma t = N_{\text{abs}}$), yields

$$\mathcal{F}_Q^{\text{TFS}} = \frac{N_{\text{abs}}^2}{\gamma^2} \sum_{ij} p_i p_j \left(\frac{1}{2} - \frac{j}{i+1+j} \right) \equiv \frac{\mathcal{G}(N_{\text{abs}})}{\gamma^2}, \quad (8)$$

with

$$p_k = \frac{(N_{\text{abs}}/2)^k e^{-N_{\text{abs}}/2}}{k!}. \quad (9)$$

For $N_{\text{abs}} \gg 1$, the Poisson distribution (9) is strongly peaked around $k = N_{\text{abs}}/2$, such that the sum in (8) is dominated by $i = j = N_{\text{abs}}/2$. In this regime, $\mathcal{G}(N_{\text{abs}}) \approx N_{\text{abs}}/2$, which is half of the upper bound (6). In contrast, as $N_{\text{abs}} \rightarrow 0$, $\mathcal{G}(N_{\text{abs}}) \approx N_{\text{abs}}^2/2$. In general, a global measurement on both modes is needed to saturate (8) [46]. The \mathcal{F}_C has been considered for more realistic photon number-resolved measurements (NRM) [45, 47–49], and we study it in the Poisson limit in the Appendix. For $g \approx 0$, we find $\mathcal{F}_C^{\text{NRM}}|_{g=0} = N_{\text{abs}}^2 e^{-N_{\text{abs}}/2}/2\gamma^2$. The exponential decay with N_{abs} can be avoided by suitably optimising over the interaction strength g , leading to a quasi-linear growth of $\mathcal{F}_C|_{g=g^*}$ with N_{abs} (see Fig. 1).

For NOON states, $\mathcal{F}_Q^{\text{NOON}}$ is given by $N^2 t^2$ times the probability of not losing any photon which, in the Poisson limit, is given by p_0^2 in (9). Hence,

$$\mathcal{F}_Q^{\text{NOON}} = \frac{N_{\text{abs}}^2}{\gamma^2} e^{-N_{\text{abs}}}. \quad (10)$$

For $N_{\text{abs}} \ll 1$, NOON perform twice as good as TFS, but this advantage is exponentially suppressed for larger N_{abs} . In fact, NOON states are optimal for $N_{\text{abs}} \ll 1$, which means that the bound (6) can not be saturated in this regime. In the regime $N_{\text{abs}} \gg 1$, the upper bound (6) can be saturated using two mode squeezed states and homodyne measurements [50, 51], which we show in the Appendix. The performance

of TFS, squeezed and NOON states in the Poisson limit is summarised in Fig. 1. It remains an interesting open question to explore whether (6) can be saturated for $N_{\text{abs}} = \mathcal{O}(1)$ for more general states, such as [52, 53], thus complementing previous results for $N_{\text{abs}} \propto N$ [43, 54–58].

Summarising, quantum photonic states (TFS, squeezed or NOON states) can provide an arbitrarily large advantage over the classical bound (5), which however requires $N \rightarrow \infty$. When N is finite with $N \gg 1$, we can use $N_{\text{abs}} \approx N\gamma t$ and $\nu = T/t$ to approximate $(\Delta g)^{-2} = \nu \mathcal{F}$ as

$$(\Delta g)^{-2} \approx (\Delta g)_{\text{coh}}^{-2} \frac{N}{N_{\text{abs}}^2} \mathcal{F}, \quad (11)$$

where \mathcal{F} is any of the CFI or QFI shown in Fig. 1. This indicates a linear increase of the quantum advantage with N . Yet, this requires perfect preparation and measurement, which motivates the analysis of noise robustness in what follows.

QUANTUM ADVANTAGE IN REALISTIC SCENARIOS

Let us consider the main practical limitations: measurement devices with efficiency $\eta < 1$ (here $1 - \eta$ is the probability of losing a photon in the measurement process), and an extra time t_{ext} to prepare and measure quantum states [18].

First, we illustrate in Fig. 2 (a) that TFS with low N can overcome the bound (5) when N_{abs} is small, even in the presence of imperfections (in the figure, we take $\eta = 0.96$ and $\gamma t_{\text{ext}} = 0.04$). Similar results are found for NRM (see Appendix). Importantly, in both cases the corresponding protocol requires measuring a finite number of samples, $\nu/T\gamma \approx N/N_{\text{abs}}$, making it feasible in practice.

Second, the robustness of such quantum advantages to finite detector efficiency (η) and extra times (t_{ext}) is analysed in Fig. 2 (b) for TFS and $N_{\text{abs}} = 1$. Whereas for $t_{\text{ext}} = 0$ or $\eta = 1$ increasing N is generally favourable, we find that TFS of low N ($N \approx 8 - 20$)

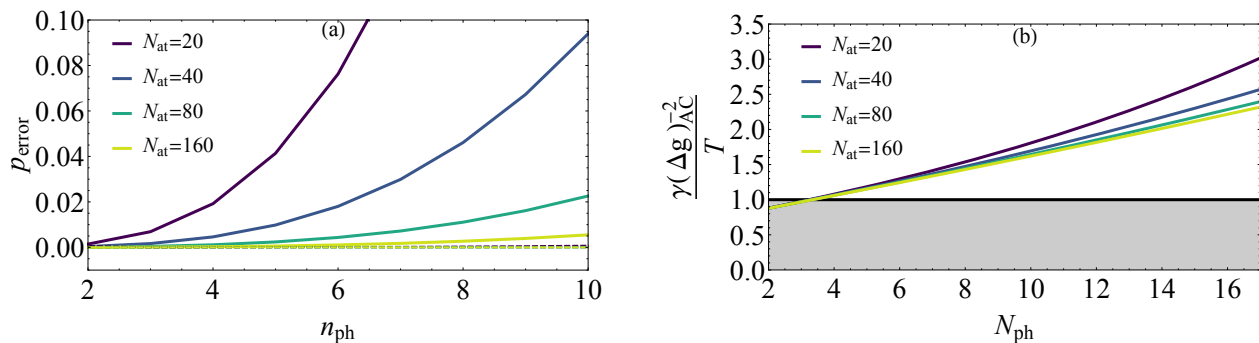


Figure 3. (a) Error probability in the absorption process, i.e., probability that the photons are not absorbed by the atoms. We take as an initial state for the cavity a Fock state with n_{ph} , which interacts with the atomic array (the atoms start in the ground state) through (12) for a time t_{meas} . In dashed lines, we show the same for two repetitions of the absorption process, leading to $p_{\text{error}} \approx 0$ (b) Measurement precision $(\Delta g)_{\text{AC}}^{-2}$ for probabilistic TFS prepared through the atom-cavity coupling at $g \approx 0$, using NRM and with $N_{\text{abs}} = 1$. Details on the calculation of $(\Delta g)_{\text{AC}}^{-2}$ are provided in the Appendix. Parameters for both plots: $J = 1$ and $\omega = 1$.

are most robust to noise when both $t_{\text{ext}} > 0$ and $1 - \eta$ are non-negligible. In particular, for TFS of $N = 8$, the quantum advantage prevails for $\eta > 0.9$ and $\gamma t_{\text{ext}} < 0.12$. In the Appendix, we provide an extended discussion of noise robustness, including upper bounds on general states. We find that, while the presence of η and t_{ext} severely restricts the maximal possible quantum advantage, the main practical conclusion of our paper remains: In frequency measurements of delicate samples, few-photon quantum states (TFS, NOON, or squeezed) can overcome classical strategies using arbitrarily intense coherent states and an arbitrarily large number of samples when N_{abs} is low (i.e. the bound Eq. (5)).

IMPLEMENTATION IN CAVITY QED

Although quantum advantages can be obtained already for low N and can tolerate imperfections (see Fig. 2 and Appendix), it is crucial to devise implementations where quantum states are prepared and measured fast, and with high efficiency. Here, we therefore outline a protocol based on cavity QED [37] or circuit QED [38] capable of generating and observing Fock states of light in cavities, inspired by recent progress on metrology and number-resolved measurements in waveguide QED [59–62]. The key idea is to engineer an interaction of the cavity with a set of resonant qubits/atoms, such that in addition to Eq. (1), the two cavities are each coupled to a collection of resonant atoms via

$$H_{\text{Dicke}} = \sum_{\alpha=a,b} \sum_i^{N_{\text{at}}} [\omega \sigma_{i,\alpha}^z + J(t)(\sigma_{i,\alpha}^- \alpha^\dagger + \text{H.c.})]. \quad (12)$$

Let us suppose that $J(t)$ can be turned on and off at will, and that it is possible to measure the collective spin of the atoms $S_\alpha^z = \sum_i \sigma_{\alpha,i}^z$.

Starting from the ground state, a photonic Fock state in each cavity is produced by exciting the atoms, allowing them to interact with the cavity, and in the

end heralding how many atoms have decayed. For a given target photon number n_{ph} , the protocol consists on: (i) Excite all atoms. (ii) The cavity-atom interaction is turned on, $J(t) = J$, for a time t_{prep} . (iii) The cavity-atom interaction is turned off and S_α^z is measured. Conditional on the measurement outcome $N_{\text{at}} - k_\alpha$, the cavity is projected in a Fock state with k_α photons, which takes place with probability $q(k_\alpha)$. This process can be done in parallel for both cavities, and on average $N_{\text{ph}} = 2n_{\text{ph}}$ photons are created. For $n_{\text{ph}} \ll N_{\text{at}}$ (linear regime), we find that $t_{\text{prep}} \approx \sqrt{n_{\text{ph}}/N_{\text{at}}} J^{-2}$ and $q(k_\alpha) \approx n_{\text{ph}}^{k_\alpha}/(n_{\text{ph}} + 1)^{k_\alpha+1}$; whereas for $n_{\text{ph}} \approx \mathcal{O}(N_{\text{at}})$ (non-linear regime) both t_{prep} and $q(k_\alpha)$ can be determined numerically by solving (12) (see Appendix for details).

After this preparation stage, we let the photonic system evolve for some time t , which is the time relevant for our discussion in the rest of the article. In the mean time, the remaining $N_{\text{at}} - k_\alpha$ atoms need to be reset to the ground state in order to prepare them for the final measurement.

To measure the final photon distribution in the cavity, we again turn on the atom-cavity coupling $J(t)$, which allows the atoms to reabsorb photons from the cavity. After a time $t_{\text{meas}} = \pi/2J\sqrt{N_{\text{at}}}$, the photons are re-absorbed with an error p_{error} of order $\mathcal{O}((n_{\text{ph}}/N_{\text{at}})^2)$, see Fig. 3 (a). If p_{error} is non-negligible, this process can be repeated which substantially reduces p_{error} ; this is also illustrated in Fig. 3. Adding up the total number of excitations observed in the measurements yields the measurement result, thus implementing a number-resolved measurement (NRM) in each cavity.

In practice, the following constraints need to be satisfied for the successful implementation of this scheme: (i) $p_{\text{error}} \ll 1$ to ensure a high detector efficiency in the NRM, and (ii) $t_{\text{ext}} = (t_{\text{prep}} + t_{\text{meas}}) \propto 1/J\sqrt{N_{\text{at}}} \ll \gamma^{-1}$, so that t_{ext} can be neglected. The linear regime where $N_{\text{at}} \gg n_{\text{ph}}$ is hence convenient for the implementation of this protocol, and it is also useful to engineer a strong atom-cavity coupling $J \gg \gamma$. Experimental requirements needed for the successful im-

plementation of this proposal are discussed in the SM, where we argue that both cavity QED [63–65] and circuit QED [66–68] appear as promising platforms.

Even when both conditions are met, the discussed preparation scheme does not produce TFS, but rather Fock states distributed according to $q(k_\alpha)$. Furthermore, the NRM in each cavity is in general not optimal for metrology, i.e., the corresponding CFI does not saturate \mathcal{F}_Q (see Fig. 1, the Appendix, and Refs. [47–49]). While both effects lead to a reduction for the quantum advantages reported in Fig. 2, we find that quantum advantages can be obtained for $N_{\text{ph}} \equiv 2n_{\text{ph}} \approx 4 - 20$, and $N_{\text{at}} \approx 20 - 100$ with the discussed implementation, as shown in Fig. 3 for $N_{\text{abs}} = 1$. Details on the calculation of $(\Delta g)_{\text{AC}}^{-2}$ for the atom-cavity (AC) implementation, as well as an analysis to robustness to non-idealities ($\eta > 1$ and $t_{\text{ext}} > 0$), is provided in the Appendix.

CONCLUSIONS

While quantum advantages in photonic metrology are well established when the (average) photon number is fixed [3–5], in specific situations, other constraints might be more meaningful. For example, when non-linear effects or quantum backaction limit the light intensity, a more sophisticated analysis has to take these effects into account [69]. Here, we study a complimentary situation, where photosensitive samples imply that the number of absorbed photons is limited [9–13, 15]. While in interferometric measurements this coincides with the traditional constraint on N , we have shown that it leads to qualitatively new results in frequency measurements. In this case, finite quantum resources for metrology (finite photon number, finite number of samples, finite time) become more powerful than infinite classical resources (unbounded photon number, unlimited number of samples, finite time). We have characterized these advantages for a model of two coupled oscillators, which can be realized in a cavity QED set-up, but our results suggest similar advantages in frequency measurements of delicate samples where photon absorption can be modelled as a Markovian process.

Acknowledgements. We thank J. Kołodyński and M. W. Mitchell for insightful discussions. M. P.-L. acknowledges funding from Swiss National Science Foundation (Ambizione PZ00P2-186067). D.M. and J.I.C. acknowledge funding from ERC Advanced Grant QENOCOBA under the EU Horizon 2020 program (Grant Agreement No. 742102).

-
- [1] V. Giovannetti, S. Lloyd, and L. Maccone, *Nature Photonics* **5**, 222 (2011).
 [2] G. Tóth and I. Apellaniz, *Journal of Physics A: Mathematical and Theoretical* **47**, 424006 (2014).
 [3] R. Demkowicz-Dobrzański, M. Jarzyna, and

- J. Kołodyński, in *Progress in Optics* (Elsevier, 2015) pp. 345–435.
 [4] J. P. Dowling and K. P. Seshadreesan, *Journal of Lightwave Technology* **33**, 2359 (2015).
 [5] E. Polino, M. Valeri, N. Spagnolo, and F. Sciarrino, arXiv preprint arXiv:2003.05821 (2020).
 [6] C. M. Caves, *Phys. Rev. D* **23**, 1693 (1981).
 [7] M. J. Holland and K. Burnett, *Phys. Rev. Lett.* **71**, 1355 (1993).
 [8] J. J. Bollinger, W. M. Itano, D. J. Wineland, and D. J. Heinzen, *Phys. Rev. A* **54**, R4649 (1996).
 [9] T. Ono, R. Okamoto, and S. Takeuchi, *Nature Communications* **4** (2013), 10.1038/ncomms3426.
 [10] M. A. Taylor, J. Janousek, V. Daria, J. Knittel, B. Hage, H.-A. Bachor, and W. P. Bowen, *Nature Photonics* **7**, 229 (2013).
 [11] M. A. Taylor, J. Janousek, V. Daria, J. Knittel, B. Hage, H.-A. Bachor, and W. P. Bowen, *Phys. Rev. X* **4**, 011017 (2014).
 [12] M. A. Taylor and W. P. Bowen, *Physics Reports* **615**, 1 (2016).
 [13] R. Whittaker, C. Erven, A. Neville, M. Berry, J. L. O’Brien, H. Cable, and J. C. F. Matthews, *New Journal of Physics* **19**, 023013 (2017).
 [14] R. Cole, *Cell Adhesion & Migration* **8**, 452 (2014).
 [15] F. Wolfgramm, C. Vitelli, F. A. Beduini, N. Godbout, and M. W. Mitchell, *Nature Photonics* **7**, 28 (2012).
 [16] S. F. Huelga, C. Macchiavello, T. Pellizzari, A. K. Ekert, M. B. Plenio, and J. I. Cirac, *Phys. Rev. Lett.* **79**, 3865 (1997).
 [17] A. Shaji and C. M. Caves, *Phys. Rev. A* **76**, 032111 (2007).
 [18] A. J. Hayes, S. Dooley, W. J. Munro, K. Nemoto, and J. Dunningham, *Quantum Science and Technology* **3**, 035007 (2018).
 [19] Y. Matsuzaki, S. C. Benjamin, and J. Fitzsimons, *Phys. Rev. A* **84**, 012103 (2011).
 [20] A. W. Chin, S. F. Huelga, and M. B. Plenio, *Phys. Rev. Lett.* **109**, 233601 (2012).
 [21] R. Chaves, J. B. Brask, M. Markiewicz, J. Kołodyński, and A. Acín, *Phys. Rev. Lett.* **111**, 120401 (2013).
 [22] J. B. Brask, R. Chaves, and J. Kołodyński, *Phys. Rev. X* **5**, 031010 (2015).
 [23] A. Smirne, J. Kołodyński, S. F. Huelga, and R. Demkowicz-Dobrzański, *Phys. Rev. Lett.* **116**, 120801 (2016).
 [24] M. J. Woolley, G. J. Milburn, and C. M. Caves, *New Journal of Physics* **10**, 125018 (2008).
 [25] M. Beau and A. del Campo, *Phys. Rev. Lett.* **119**, 010403 (2017).
 [26] M. Naghiloo, A. N. Jordan, and K. W. Murch, *Phys. Rev. Lett.* **119**, 180801 (2017).
 [27] S. Pang and A. N. Jordan, *Nature Communications* **8** (2017), 10.1038/ncomms14695.
 [28] L. Sun, X. He, C. You, C. Lv, B. Li, S. Lloyd, and X. Wang, arXiv preprint arXiv:2004.01216 (2020).
 [29] U. Dörner, *New Journal of Physics* **14**, 043011 (2012).
 [30] W. Dür, M. Skotiniotis, F. Fröwis, and B. Kraus, *Phys. Rev. Lett.* **112**, 080801 (2014).
 [31] E. M. Kessler, I. Lovchinsky, A. O. Sushkov, and M. D. Lukin, *Phys. Rev. Lett.* **112**, 150802 (2014).
 [32] G. Arrad, Y. Vinkler, D. Aharonov, and A. Retzker, *Phys. Rev. Lett.* **112**, 150801 (2014).
 [33] B. Escher, R. de Matos Filho, and L. Davidovich, *Nature Physics* **7**, 406 (2011).
 [34] R. Demkowicz-Dobrzański, J. Kołodyński, and M. Guță, *Nature Communications* **3** (2012), 10.1038/ncomms2067.

- [35] J. Kolodyński and R. Demkowicz-Dobrzański, *New Journal of Physics* **15**, 073043 (2013).
- [36] S. I. Knysh, E. H. Chen, and G. A. Durkin, arXiv preprint arXiv:1402.0495 (2014).
- [37] S. Haroche and J.-M. Raimond, *Exploring the Quantum*, Vol. 5 (Oxford University Press, 2006) p. 11.
- [38] A. Blais, S. M. Girvin, and W. D. Oliver, *Nature Physics* **16**, 247 (2020).
- [39] C. W. Helstrom, *Quantum Detection and Estimation Theory* (Elsevier Science, 1976).
- [40] A. S. Holevo, *Probabilistic and Statistical Aspects of Quantum Theory (Statistics & Probability) (English and Russian Edition)* (Elsevier Science, 1982).
- [41] S. L. Braunstein and C. M. Caves, *Phys. Rev. Lett.* **72**, 3439 (1994).
- [42] A. Fujiwara and H. Imai, *Journal of Physics A: Mathematical and Theoretical* **41**, 255304 (2008).
- [43] S. Knysh, V. N. Smelyanskiy, and G. A. Durkin, *Phys. Rev. A* **83**, 021804 (2011).
- [44] R. A. Campos, C. C. Gerry, and A. Benmoussa, *Phys. Rev. A* **68**, 023810 (2003).
- [45] A. Datta, L. Zhang, N. Thomas-Peter, U. Dorner, B. J. Smith, and I. A. Walmsley, *Phys. Rev. A* **83**, 063836 (2011).
- [46] M. G. A. Paris, *International Journal of Quantum Information* **07**, 125 (2009).
- [47] T. Kim, O. Pfister, M. J. Holland, J. Noh, and J. L. Hall, *Phys. Rev. A* **57**, 4004 (1998).
- [48] L. Pezzé and A. Smerzi, *Phys. Rev. Lett.* **110**, 163604 (2013).
- [49] W. Zhong, Y. Huang, X. Wang, and S.-L. Zhu, *Phys. Rev. A* **95**, 052304 (2017).
- [50] B. Yurke, S. L. McCall, and J. R. Klauder, *Phys. Rev. A* **33**, 4033 (1986).
- [51] S. Olivares and M. G. A. Paris, *Optics and Spectroscopy* **103**, 231 (2007).
- [52] D. Šafránek and I. Fuentes, *Phys. Rev. A* **94**, 062313 (2016).
- [53] T. Matsubara, P. Facchi, V. Giovannetti, and K. Yuasa, *New Journal of Physics* **21**, 033014 (2019).
- [54] S. D. Huver, C. F. Wildfeuer, and J. P. Dowling, *Phys. Rev. A* **78**, 063828 (2008).
- [55] U. Dorner, R. Demkowicz-Dobrzański, B. J. Smith, J. S. Lundeen, W. Wasilewski, K. Banaszek, and I. A. Walmsley, *Phys. Rev. Lett.* **102**, 040403 (2009).
- [56] R. Demkowicz-Dobrzański, U. Dorner, B. J. Smith, J. S. Lundeen, W. Wasilewski, K. Banaszek, and I. A. Walmsley, *Phys. Rev. A* **80**, 013825 (2009).
- [57] H. Cable and G. A. Durkin, *Phys. Rev. Lett.* **105**, 013603 (2010).
- [58] J. Calsamiglia, B. Gendra, R. Muñoz-Tapia, and E. Bagan, *New Journal of Physics* **18**, 103049 (2016).
- [59] A. González-Tudela, V. Paulisch, H. J. Kimble, and J. I. Cirac, *Phys. Rev. Lett.* **118**, 213601 (2017).
- [60] V. Paulisch, M. Perarnau-Llobet, A. González-Tudela, and J. I. Cirac, *Phys. Rev. A* **99**, 043807 (2019).
- [61] M. Perarnau-Llobet, A. González-Tudela, and J. I. Cirac, *Quantum Science and Technology* **5**, 025003 (2020).
- [62] D. Malz and J. I. Cirac, arXiv preprint arXiv:1906.12296 (2019).
- [63] H. Zhang, R. McConnell, S. Ćuk, Q. Lin, M. H. Schleier-Smith, I. D. Leroux, and V. Vuletić, *Physical Review Letters* **109**, 133603 (2012).
- [64] D. B. Hume, I. Stroescu, M. Joos, W. Muessel, H. Strobel, and M. K. Oberthaler, *Physical Review Letters* **111**, 253001 (2013), arXiv:1307.7598.
- [65] F. Haas, J. Volz, R. Gehr, J. Reichel, and J. Esteve, *Science* **344**, 180 (2014).
- [66] E. Jeffrey, D. Sank, J. Y. Mutus, T. C. White, J. Kelly, R. Barends, Y. Chen, Z. Chen, B. Chiaro, A. Dunsworth, A. Megrant, P. J. J. O'Malley, C. Neill, P. Roushan, A. Vainsencher, J. Wenner, A. N. Cleland, and J. M. Martinis, *Physical Review Letters* **112**, 190504 (2014).
- [67] T. Walter, P. Kurpiers, S. Gasparinetti, P. Magnard, A. Potočnik, Y. Salathé, M. Pechal, M. Mondal, M. Oppliger, C. Eichler, and A. Wallraff, *Physical Review Applied* **7**, 054020 (2017).
- [68] R. Dassonneville, T. Ramos, V. Milchakov, L. Planat, Dumur, F. Foroughi, J. Puertas, S. Leger, K. Bharadwaj, J. Delaforce, C. Naud, W. Hasch-Guichard, J. J. García-Ripoll, N. Roch, and O. Buisson, *Physical Review X* **10**, 11045 (2020).
- [69] M. W. Mitchell, *Quantum Science and Technology* **2**, 044005 (2017).
- [70] R. J. Thompson, G. Rempe, and H. J. Kimble, *Physical Review Letters* **68**, 1132 (1992).
- [71] M. Brune, F. Schmidt-Kaler, A. Maali, J. Dreyer, E. Hagley, J. M. Raimond, and S. Haroche, *Physical Review Letters* **76**, 1800 (1996).
- [72] T. Yoshie, A. Scherer, J. Hendrickson, G. Khitrova, H. M. Gibbs, G. Rupper, C. Ell, O. B. Shchekin, and D. G. Deppe, *Nature* **432**, 200 (2004).
- [73] A. Wallraff, D. I. Schuster, A. Blais, L. Frunzio, R.-S. Huang, J. Majer, S. Kumar, S. M. Girvin, and R. J. Schoelkopf, *Nature* **431**, 162 (2004).
- [74] J. P. Reithmaier, G. Sęk, A. Löffler, C. Hofmann, S. Kuhn, S. Reitzenstein, L. V. Keldysh, V. D. Kulakovskii, T. L. Reinecke, and A. Forchel, *Nature* **432**, 197 (2004).
- [75] I. Chiorescu, P. Bertet, K. Semba, Y. Nakamura, C. J. P. M. Harmans, and J. E. Mooij, *Nature* **431**, 159 (2004).

Squeezed states

Squeezed states also enable Heisenberg scaling [50, 51], and hence can provide a finite amount of information in the Poisson limit $t \rightarrow 0$ and $N \rightarrow \infty$. This is explored in this section.

We take as an initial state a vacuum-squeezed state together with a coherent-squeezed state: $|\phi_0\rangle = D_a(\alpha)S_a(s)S_b(r)|0\rangle$ with $D_a(\alpha) = e^{-\alpha(a^\dagger - a)}$, and $S_y(x) = e^{\frac{x}{2}(y^2 - (y^\dagger)^2)}$, $x = s, r$ and $y = a, b$; and we take $\alpha, r > 0$ and $s < 0$. The average total number of photons is:

$$N = \alpha^2 + \sinh^2 r + \sinh^2 s, \quad (13)$$

and it is convenient to define: $\beta_x = \sinh^2 x/N$, $x = r, s$. We consider homodyne measurements in the output states. Following [51], the \mathcal{F}_C in the regime $N \gg 1$ is given by (the extra factor t^2 comes from the fact that we

are measuring a frequency):

$$\mathcal{F}_C^{\text{sq}} = \frac{N^2 t^2 (1 - 2\beta_r)^2}{N \frac{1 - e^{-\gamma t}}{e^{-\gamma t}} + \frac{1}{4} \left(\frac{1}{\beta_r} + \frac{\beta_r}{\beta_s} - 3 \right)}. \quad (14)$$

Taking the Poisson limit ($t \rightarrow 0$ with $Nt\gamma = N_{\text{abs}}$), leads to

$$\mathcal{F}_C^{\text{sq}} = \frac{N_{\text{abs}}^2}{\gamma^2} \frac{4(1 - 2\beta_r)^2}{4N_{\text{abs}} + (\beta_r^{-1} + \beta_r 2\beta_s^{-1} - 3)}. \quad (15)$$

At this point one can maximise this expression with respect to β_x , with the constraints $0 < \beta_x < 1$ and $\beta_a + \beta_b \leq 1$, in order to optimise the measurement precision. For $N_{\text{abs}} \ll 1$, we find that $\mathcal{F}_C^{\text{sq}} \approx N_{\text{abs}}^2 / \gamma^2$, hence squeezed states perform close to NOON states in this regime. On the other hand, for $N_{\text{abs}} \gg 1$, we have $\mathcal{F}_C^{\text{sq}} \approx N_{\text{abs}} / \gamma^2$, thus saturating the upper bound presented in the main text. For intermediate values of N_{abs} , a numerical optimisation is presented in Fig. 1 of the main text. It remains an interesting question whether more generalised Gaussian states and/or measurement schemes [52, 53] can outperform this proposal in this regime.

Classical Fisher Information for number-resolved measurements

In this section we compute the classical Fisher information,

$$\mathcal{F}_C = \sum_j \frac{1}{q_j} \dot{q}_j^2, \quad (16)$$

where q_j is the probability to obtain outcome j , for number resolved measurements in the set-up described in the main text. Because of the map between our framework and Mach-Zehnder interferometry with symmetric (time-dependent) photon loss, we can follow similar derivations in that context, see e.g. Refs. [47–49]. Let us first compute the probabilities of the photon-number measurements for the initial Fock state $|k, m\rangle$ and unitary $U_g = e^{-itH_0} e^{-itH_{\text{int}}}$. First of all we note that e^{-itH_0} commutes with the initial state (with a well defined photon number in each arm) and hence can be ignored for the number-resolved statistics. We first compute:

$$P(k, m, q, g) \equiv |\langle k - q, m + q | e^{-igtH_{\text{int}}} |k, m\rangle|^2 \quad (17)$$

with $|k, m\rangle = \frac{1}{\sqrt{k!m!}} (a^\dagger)^k (b^\dagger)^m |0, 0\rangle$ and $q \in [-m, k]$. Noting that:

$$\begin{aligned} a_g^\dagger &\equiv e^{-igtH_{\text{int}}} a^\dagger e^{igtH_{\text{int}}} = a^\dagger \cos\left(\frac{tg}{2}\right) + ib^\dagger \sin\left(\frac{tg}{2}\right) \\ b_g^\dagger &\equiv e^{-igtH_{\text{int}}} b^\dagger e^{igtH_{\text{int}}} = b^\dagger \cos\left(\frac{tg}{2}\right) + ia^\dagger \sin\left(\frac{tg}{2}\right), \end{aligned} \quad (18)$$

we obtain

$$P(k, m, q, g) = \frac{(m+q)!(k-q)!}{m!k!} (\tan\theta)^{2q} \left(\sum_{j=0}^m \binom{m}{j} \binom{k}{j+q} (-1)^j (\cos\theta)^{k+m-2j} (\sin\theta)^{2j} \right)^2 \quad (19)$$

where we defined $\theta \equiv tg/2$, and $q \in [-m, k]$. This can also be expressed as:

$$\begin{aligned} P(k, m, q, g) &= \frac{(m+q)!(k-q)!}{m!k!} (\tan\theta)^{2q} \\ &\left((-1)^k \binom{m}{k+1} \binom{k}{k+q+1} \frac{(\sin\theta)^{2k+2}}{(\cos\theta)^{2-m-k}} {}_3F_2(1, -m+k+1, q+1; k+2, k+q+2; -\tan^2(\theta)) \right. \\ &\left. + \binom{k}{q} (\cos\theta)^{m+k} {}_2F_1(-m, q-k; q+1; -\tan^2(\theta)) \right)^2, \end{aligned} \quad (20)$$

where ${}_pF_q(a; b; z)$ is the generalized hypergeometric function.

Next, we compute the probability to obtain outcomes $\{k, m\}$ for the state:

$$\rho = \sum_{k,j} p_k p_j |n-k, n-j\rangle \langle n-k, n-j| \quad (21)$$

with

$$p_k = \mu^k (1 - \mu)^{n-k} \binom{n}{k}, \quad \mu = 1 - e^{-\gamma t}. \quad (22)$$

It is convenient to introduce:

$$\begin{aligned} n_{\text{loss}} &\equiv 2n - (k + m) \\ q &\equiv n - k \end{aligned} \quad (23)$$

Then, we have for (21)

$$P^{\text{Fock}}(n_{\text{loss}}, q, g) = \sum_{l=0}^{n_{\text{loss}}} p_l p_{n_{\text{loss}}-l} P(n-l, n+l-n_{\text{loss}}, q-l, g) \quad (24)$$

The only remaining step is to compute the classical Fisher information using (16):

$$\mathcal{F}_C^{\text{TFS}}(g) = \sum_{n_{\text{loss}}=0}^{2n} \sum_{q=n_{\text{loss}}-n}^n \frac{(\partial_g P^{\text{Fock}}(n_{\text{loss}}, q, g))^2}{P^{\text{Fock}}(n_{\text{loss}}, q, g)} \quad (25)$$

To gain some analytical insight for this expression, we can compute it in the limit $g \rightarrow 0$. Following [48, 61], we can expand the probabilities around $g \approx 0$ up to order $\mathcal{O}(g^2)$, and realise that only instances where $n+1$ photons are measured in one of the modes contribute to the CFI. This leads to the following analytical expression for the CFI [45]:

$$\lim_{g \rightarrow 0} \mathcal{F}_C^{\text{TFS}}(g) = 2t^2(n+1)n(1-\mu)^{n+1}, \quad (26)$$

which shows an exponential decay with $n = N/2$. This is hence far from \mathcal{F}_Q for large N , while still better than NOON states. For future convenience, we also give the corresponding expression when the initial state is $\rho = \sum_{k,j} p_k p_j |n-k, m-j\rangle \langle n-k, m-j|$:

$$\lim_{g \rightarrow 0} \mathcal{F}_C^{n,m}(g) = t^2 \left((1-\mu)^{n+1}(n+1)m + (1-\mu)^{m+1}(m+1)n \right). \quad (27)$$

Finally, we numerically compute (25) for different g , μ and N for the state (21) (and setting $t = 1$). An example is shown in Fig. 4, from it we see that in general the dependence of \mathcal{F}_C with g is non-trivial, and so is the point where it is maximized. The figure also shows that indeed (16) does not saturate \mathcal{F}_Q for number-resolved measurements. In Fig. 4 we also show (25) as a function of N , where it becomes apparent the importance of maximizing \mathcal{F}_C with respect to g for the number-resolved-measurements as N increases. The numerical results suggest that a systematic improvement with respect to the Shot-Noise-Limit can be obtained for any N with suitably optimized number-resolved-measurements.

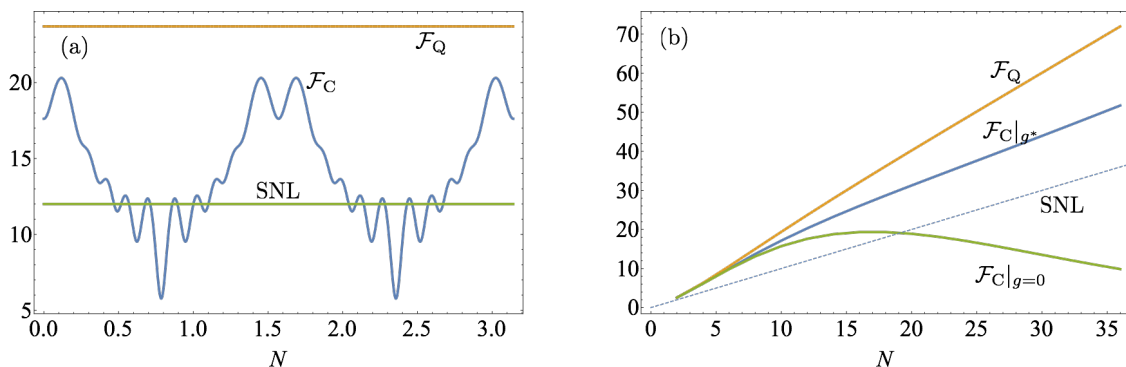


Figure 4. (a) CFI, QFI, and SNL vs ϕ . Parameters: $N = 12$, $\mu = 0.2$, and $t = 1$. (b) \mathcal{F}_Q and \mathcal{F}_C vs N for $\mu = 0.2$ and $t = 1$.

Let us now look at the Poisson limit $N \rightarrow \infty$, $t \rightarrow 0$ while satisfying $2\gamma tn \rightarrow N_{\text{abs}}$. First, from (26), we can study the Poisson limit $2\gamma tn \rightarrow N_{\text{abs}}$, where we obtain:

$$\lim_{g \rightarrow 0} \mathcal{F}_C^{\text{TFS}} = \frac{N_{\text{abs}}^2}{2\gamma^2} e^{-N_{\text{abs}}/2}. \quad (28)$$

To obtain similar analytical expression for arbitrary g is challenging due to the complexity of obtaining asymptotic expressions for the generalized hypergeometric functions. Yet, we can obtain numerical results for rather large $N \approx 100 - 1000$. To do this, it is useful to approximate \mathcal{F}_C in (25) as:

$$\mathcal{F}_C^{\text{TFS}}(g) \approx \sum_{n_{\text{loss}}=0}^{N_{\text{loss}}^{\text{max}}} \sum_{q=-q_{\text{max}}}^{q_{\text{max}}} \frac{(\partial_g P^{\text{Fock}}(n_{\text{loss}}, q, g))^2}{P^{\text{Fock}}(n_{\text{loss}}, q, g)} \quad (29)$$

since only terms with $q = \mathcal{O}(1)$ and $N_{\text{loss}}^{\text{max}} = \mathcal{O}(N_{\text{abs}})$ contribute to the sum in the Poisson limit (other terms are exponentially small). In our numerical simulations, we take $q_{\text{max}} = 10$ and $N_{\text{loss}}^{\text{max}} = 4N_{\text{abs}}$, and the results become in practice indistinguishable when these parameters are varied. Numerical results are shown in Fig. 2 of the main text.

Optimal measurement

Finally, we note that the optimal measurement L where the classical Fisher info (16) saturates Q is given by [46]:

$$\begin{aligned} L &= i \sum_{k,l} \frac{\tilde{p}_k \tilde{p}_l - \tilde{p}_{k-1} \tilde{p}_{l+1}}{\tilde{p}_k \tilde{p}_l + \tilde{p}_{k-1} \tilde{p}_{l+1}} \sqrt{k(l+1)} \left(|k, l\rangle \langle k-1, l+1| + |l, k\rangle \langle l+1, k-1| \right) \\ &= i \sum_{k,l} \frac{(n-k+1)(l+1) - k(n-l)}{n(l+k+1) + k(n-l)} \sqrt{k(l+1)} \left(|k, l\rangle \langle k-1, l+1| + |l, k\rangle \langle l+1, k-1| \right). \end{aligned} \quad (30)$$

with $\tilde{p}_k = p_{n-k}$. In the presence of photon loss (i.e. $p_0 \neq 1$), this does not correspond to a number resolved measurement of the two modes, but to a global measurement involving both modes.

Robustness to imperfections: Photon loss in the detection process and finite time for preparation and measurement of quantum states

In this section, we discuss how $(\Delta g)^{-2} \equiv \nu \mathcal{F}$ of general quantum states decreases due to: finite N , photon loss in the measurement process, and an extra-time t_{ext} of preparation/measurement of quantum resources. We then also discuss the particular case of twin Fock states (TFS), both with optimal measurements ($\mathcal{F}_C^{\text{TFS}}$) and with photon number-resolved measurements (NRM) ($\mathcal{F}_C^{\text{TFS}}$).

More precisely, we model photon loss in the measurement process through a beamsplitter interaction with vacuum of each mode a, b :

$$\begin{aligned} a &\rightarrow \sqrt{\eta}a + \sqrt{1-\eta}e_1 \\ b &\rightarrow \sqrt{\eta}b + \sqrt{1-\eta}e_2 \end{aligned} \quad (31)$$

so that there is a probability $1 - \eta$ of losing a photon. Since η is the same in both modes, this beam splitter interaction commutes with H_{int} , so that this operation can be applied either before (imperfect state preparation) or after (imperfect detector) the acquisition of information of g . In particular, we can generalise μ defined in the main text as:

$$\mu = 1 - e^{-\gamma t} \eta, \quad (32)$$

where η is independent of the time of the process, and where we recall that $N_{\text{abs}} = N(1 - e^{-\gamma t})$ (i.e. the photons loss in the vacuum do not damage the sample). Indeed, η quantifies the efficiency of the detector.

On the other hand, we also assume the existence of an extra time t_{ext} to prepare and measure quantum states of light. The time of the process is hence generalised to:

$$T = \nu(t + t_{\text{ext}}), \quad (33)$$

where t is the time used in the interference process.

We start by giving general bounds on $\nu \mathcal{F}_Q$ for any quantum state given different constraints:

- *Finite N .* Let us first assume finite N , but $\eta = 1$ and $t_{\text{ext}} = 0$. Using the upper bound of [33–35, 42, 43], we have:

$$\mathcal{F}_Q \leq t^2 N \frac{e^{-\gamma t}}{1 - e^{-\gamma t}} \leq \frac{tN}{\gamma}, \quad (34)$$

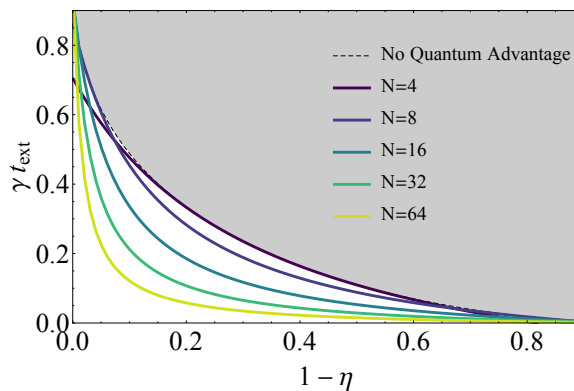


Figure 5. Here we illustrate regions where quantum advantages become possible in principle. For that, we plot the values of $\{t_{\text{ext}}, 1 - \eta\}$ for which the upper bound $\mathcal{J}(t)$, defined in (40), satisfies $\mathcal{J}(t) = 1$. Recall that if $\mathcal{J}(t) < 1$ then no quantum advantage is possible (using any state). This is shown in grey, by maximising (40) over any t (and hence N). On the other hand, for the different colourful curves t is fixed implicitly by $N_{\text{abs}} = N(1 - e^{-\gamma t})$, which provide upper bounds for a state with N photons.

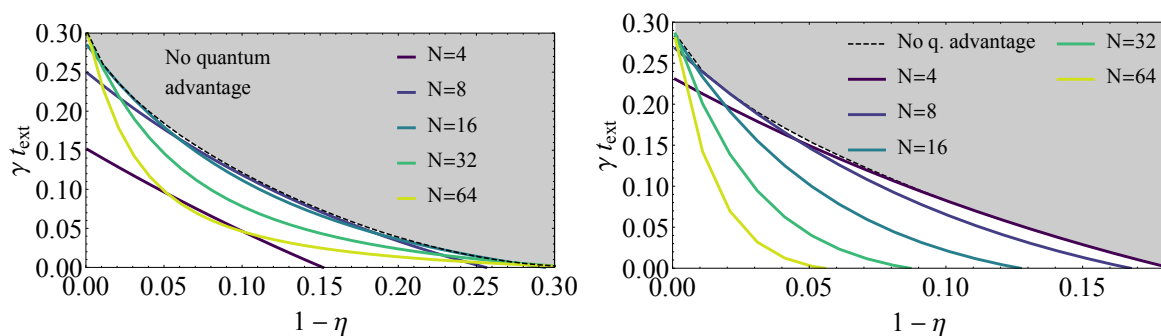


Figure 6. Similarly to Fig. 5, we plot the values $\{1 - \eta, t_{\text{ext}}\}$ for which $(\Delta g)_{\text{coh}}^{-2} / (\Delta g)_{\text{TFS}}^{-2} = 1$ (left) or $(\Delta g)_{\text{coh}}^{-2} / (\Delta g)_{\text{NRM}}^{-2} = 1$ (right) for TFS of different N and $N_{\text{abs}} = 1$. In other words, lower values of $\{1 - \eta, t_{\text{ext}}\}$ enable quantum advantages with TFS. For NRM, we consider $g \approx 0$.

where the factor t^2 comes from the fact that we are measuring a frequency-like quantity. Considering now $\nu = T/t$ measurements, we obtain:

$$(\Delta g)_N^{-2} \equiv \nu \mathcal{F}_{\mathcal{Q}} \leq \frac{TN}{\gamma} = \frac{N}{N_{\text{abs}}} (\Delta g)_{\text{coh}}^{-2}. \quad (35)$$

Since any $\eta < 1$ or $t_{\text{ext}} > 0$ can only decrease $(\Delta g)_N^{-2}$, this bound also holds for any η and t_{ext} .

- *Photon loss.* Let us now assume $0 < \eta < 1$. The starting point is now: $\mathcal{F}_{\mathcal{Q}} \leq t^2 N \eta e^{-\gamma t} / (1 - \eta e^{-\gamma t})$, which implies for the whole process with $\nu = T/t$ measurements:

$$(\Delta g)_\eta^{-2} \equiv \nu \mathcal{F}_{\mathcal{Q}} \leq T \eta N_{\text{abs}} \frac{te^{-\gamma t}}{(1 - e^{-\gamma t})(1 - \eta e^{-\gamma t})}, \quad (36)$$

which we expressed in terms of the constants T and N_{abs} . The right hand side of (36) is maximised for $t \rightarrow 0$ (or equivalently $N \rightarrow \infty$), leading to the bound:

$$(\Delta g)_\eta^{-2} \leq (\Delta g)_{\text{coh}}^{-2} \frac{\eta}{1 - \eta}. \quad (37)$$

Hence the quantum advantage comes in the form of a better prefactor $\eta/(1 - \eta)$. This prefactor advantage takes the same form as the one obtained in noisy photon interferometry when comparing coherent and quantum states with a fixed N [33–35, 42, 43].

- *Extra time.* Let us now assume an extra time t_{ext} necessary to prepare and measure using quantum resources. Let us consider the extreme case $t_{\text{ext}} > 0$ but $\eta = 1$ and no constraints on N . Taking $\eta = 1$, we have:

$$(\Delta g)_{t_{\text{ext}}}^{-2} \equiv \nu \mathcal{F}_{\mathcal{Q}} \leq TN_{\text{abs}} \frac{t^2 e^{-\gamma t}}{(t + t_{\text{ext}})(1 - e^{-\gamma t})^2}. \quad (38)$$

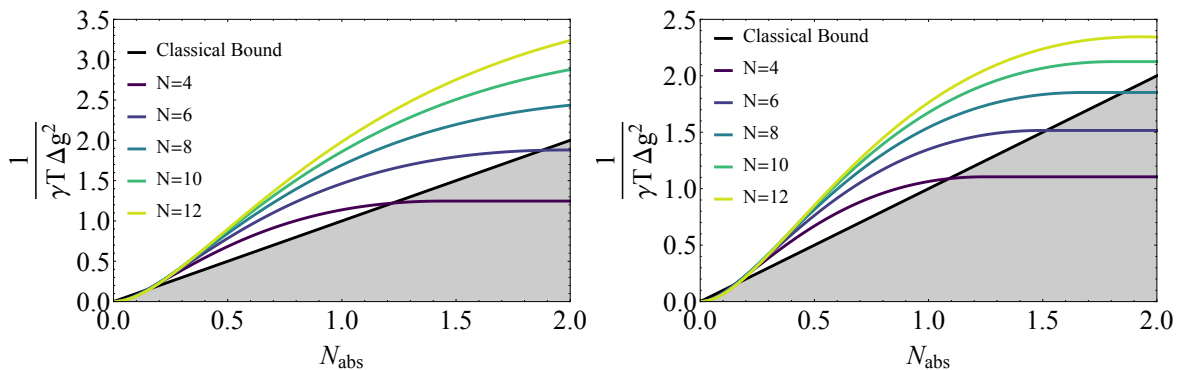


Figure 7. Plot of $(\Delta g)_{\text{TFS}}^{-2} = 1$ (left) and $((\Delta g)_{\text{NRM}}^{-2} = 1$ as a function of N_{abs} for TFS of different N . For NRM, we consider $g \approx 0$. We take $\eta = 0.95$ and $\gamma t_{\text{ext}} = 0.05$

This expression is again optimised in the limit $t \rightarrow 0$ (and hence $N \rightarrow \infty$), yielding:

$$(\Delta g)_{t_{\text{ext}}}^{-2} \leq (\Delta g)_{\text{coh}}^{-2} \frac{1}{\gamma t_{\text{ext}}}. \quad (39)$$

Let us now consider the general case where $0 < \eta < 1$ and $t_{\text{ext}} > 0$. In general we have,

$$\frac{(\Delta g)_{t_{\text{ext}}, \eta}^{-2}}{(\Delta g)_{\text{coh}}^{-2}} \leq \frac{\gamma t^2 \eta e^{-\gamma t}}{(t + t_{\text{ext}})(1 - e^{-\gamma t})(1 - \eta e^{-\gamma t})} \equiv \mathcal{J}(t). \quad (40)$$

This expression is no longer optimised in general at $t \rightarrow 0$, and in fact it does not allow for an analytical solution. We can still solve it numerically for any value of the desired value of $\mathcal{J}(t)$, which provides an upper bound on the quantum advantage. In particular, a quantum advantage is impossible if $\mathcal{J}(t) = 1 \forall t$. This condition is plot in Fig. 5, where we compute the values of η, t_{ext} for which $\max_t \mathcal{J}(t) = 1$. In Fig. 5, we also plot the values η, t_{ext} for which $\max_t \mathcal{J}(t) = 1$ but by fixing t implicitly by $N_{\text{abs}} = N(1 - e^{-\gamma t})$, which provide upper bounds for a state with N photons. Interestingly, we find that the upper bound becomes more robust to noise in the regime where both t_{ext} and $1 - \eta$ are not close to zero. This suggests that in realistic implementations few-photon quantum states are desirable when N_{abs} is low.

Let us now move to the particular case of TFS by considering $(\Delta g)_{\text{TFS}}^{-2} \equiv \max_{\nu} (\nu \mathcal{F}_{\text{Q}}^{\text{TFS}})$ and $(\Delta g)_{\text{TFS}}^{-2} \equiv \max_{\nu} (\mathcal{F}_{\text{C}}^{\text{TFS}})$. It is useful to point out that, as long as $N_{\text{abs}} \leq N_{\text{abs}}^*$ (N_{abs}^* needs to be determined in each case, e.g., numerically), $\nu \mathcal{F}_{\text{Q}}^{\text{TFS}}$ (and $\nu \mathcal{F}_{\text{C}}^{\text{TFS}}$) is maximised by testing each sample until it is damaged, that is:

$$T = t\nu$$

$$t = \frac{-1}{\gamma} \ln \left(1 - \frac{N_{\text{abs}}}{N} \right) \approx \frac{N_{\text{abs}}}{\gamma N} \quad (41)$$

for $N_{\text{abs}} \leq N_{\text{abs}}^*$ (otherwise, the choice (41) is taken with $N_{\text{abs}} = N_{\text{abs}}^*$). Given this choice, we first analyse the regions where quantum advantages are possible using TFS, which is shown in Fig. 5. As expected, the regions are more restrictive than for the upper bound shown in Fig. 6. On the other hand, an example of the quantum advantage as a function of N_{abs} for different TFS and with $\eta = 0.95$ and $\gamma t_{\text{ext}} = 0.05$ is presented in Fig. 7. Similar results are obtained when considering $\mathcal{F}_{\text{C}}^{\text{TFS}}$ with NRM, which is in general lower than $\mathcal{F}_{\text{C}}^{\text{TFS}}$ as expected from Fig. 4. This is shown in both Figs. 6 and 7 by considering $g \approx 0$.

Implementation in Cavity QED

In this section we discuss the implementation in cavity QED, and in particular how to compute the measurement precision (both QFI and CFI).

Preparation stage

Initially, each cavity is set to the ground state ($n_{\text{ph}} = 0$), and all atoms N_{at} ($\alpha = a, b$) in the atomic arrays are excited. Through the atom-cavity (AC) Dicke interaction (Eq. (12) in the main text), the excitations are transformed into photons in the cavity. In general, we diagonalize exactly Eq. (12) to find the photon

distribution $q(k)$. Yet, here we provide an analytical solution in the linear regime where $n_{\text{ph}} \ll N_{\text{at}}$, which is very relevant for the implementation.

Assuming that $n_{\text{ph}} \ll N_{\text{at}}$ along the process, we can linearize the spin operator around the state with all atoms excited, obtaining $\sum_i \sigma_{\alpha}^- \simeq \sqrt{N_{\text{at}}} c_{\alpha}^{\dagger}$, where c_{α} is a bosonic annihilation operator. Thus, Eq. (12) transforms into

$$H_{\text{Dicke}} \simeq \sum_{\alpha=a,b} \sum_{i=1}^{N_{\text{at}}} [\omega \sigma_{i,\alpha}^z + (J(t) \sqrt{N_{\text{at}}} c_{\alpha}^{\dagger} \alpha^{\dagger} + \text{H.c.})]. \quad (42)$$

The time evolution is therefore a two-mode squeezing operation

$$e^{-iHt} = e^{-\zeta \alpha^{\dagger} c^{\dagger} + \text{H.c.}}, \quad \zeta = i \sqrt{N_{\text{at}}} J t = r e^{i\phi}. \quad (43)$$

Under this evolution,

$$\begin{aligned} \langle \alpha^{\dagger} \alpha \rangle &= \sinh^2 r = \sinh^2(\sqrt{N_{\text{at}}} J t) \\ \langle \alpha^{\dagger} \alpha^{\dagger} \alpha \alpha \rangle &= \sinh^2(r) [\cosh(2r) - \sinh^2(r)]. \end{aligned} \quad (44)$$

In particular, the optimal time scale to obtain n_{ph} photons is

$$t_{\text{prep}} = \frac{\sinh^{-1}(\sqrt{n_{\text{ph}}})}{\sqrt{N_{\text{at}}} J}. \quad (45)$$

On the other hand, the probability of obtaining k_{α} photons in one cavity at time t is given by: $q(k_{\alpha}) = (\tanh \sqrt{N_{\alpha}} J t)^{2k_{\alpha}} / (\cosh \sqrt{N_{\alpha}} J t)^2$. For the optimal time (45), it reads:

$$q(k_{\alpha}) \approx \frac{n_{\text{ph}}^{k_{\alpha}}}{(n_{\text{ph}} + 1)^{k_{\alpha} + 1}}, \quad (46)$$

which we recall holds in the regime $N_{\text{at}} \gg n_{\text{ph}}$.

As explained in the main text, the idea of the protocol is then as follows.

1. Let cavities and atomic arrays interact for t_{prep} .
2. Measure the number of excited atoms in each atomic array, which yields the result $N_{\text{at}} - k_{\alpha}$ with probability $q(k_{\alpha})$ ($\alpha = a, b$).
3. The measurement heralds a Fock state in the cavity with known photon number k_{α} . This Fock state is the initial state of the measurement.

Interference process and measurement precision

Indeed, at each run of the experiment, the initial state is a Fock state: $|m, l\rangle$, where the photon number m, l are known. The interaction time $t_{m,l}$ between cavities is taken such that given m, l initial photons, at most N_{abs} photons are absorbed, i.e.:

$$N_{\text{abs}} = (m + l)(1 - e^{-\gamma t_{m,l}}). \quad (47)$$

We then repeat the experiment until the accumulated time $\sum_{m,l} \nu_{m,l} t_{m,l}$ reaches T , where T is the maximal time of the protocol. We assume the total time T and N_{abs} to be limited. We are interested in the regime $\nu \equiv \sum_{m,l} \nu_{m,l} \gg 1$ (i.e. $T/t_{m,l} \gg 1$), where the statistics are dominated by typical sequences in which $\nu_{m,l} = q(m)q(l)\nu$ which, together with $T = \sum_{m,l} \nu_{m,l} t_{m,l}$, provides ν .

Assuming a large number of runs of the experiment $\nu \gg 1$ (so that enough statistics for each m, l are obtained), the measurement uncertainty $(\Delta g)^{-2}$ is bounded by

$$(\Delta g)_{\text{AC},\mathcal{Q}}^{-2} \equiv \sum_{m,l} \nu_{m,l} \mathcal{F}_{\mathcal{Q}}^{m,l} = \frac{T}{\sum_{m,l} q(m)q(l)t_{m,l}} \sum_{m,l} q(m)q(l) \mathcal{F}_{\mathcal{Q}}^{m,l} \quad (48)$$

with $\mathcal{F}_{\mathcal{Q}}^{m,l}$ is the QFI for an initial Fock state $|m, l\rangle$, and it reads (following the same reasoning provided in the main text):

$$\mathcal{F}_{\mathcal{Q}}^{m,l} = 2t_{m,l}^2 \sum_i^l \sum_j^m p_{i,l} p_{j,m} \left[(l-i)(m-j+1) \left(\frac{1}{2} - \frac{1}{1 + \frac{(m-j+1)(i+1)}{j(l-i)}} \right) + (m-j)(l-i+1) \left(\frac{1}{2} - \frac{1}{1 + \frac{(l-i+1)(j+1)}{i(m-j)}} \right) \right]. \quad (49)$$

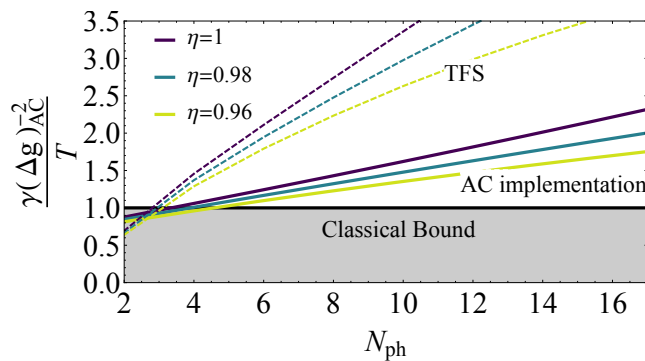


Figure 8. Plot of $(\Delta g)_{AC}^{-2} = 1$ for TFS (dashed) and the atom-cavity (AC) implementation (solid lines) as a function of n_{ph} , and given different values of η (we take $t_{ext} = 0$). We take $N_{at} = 100$ for the AC implementation, and for both cases we consider NRM with $g \approx 0$.

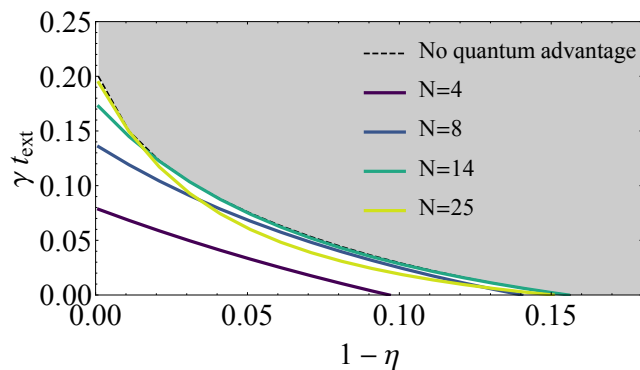


Figure 9. We plot the values $\{\eta, t_{ext}\}$ for which $(\Delta g)_{coh}^{-2}/(\Delta g)_{AC}^{-2} = 1$ given different values of n_{ph} , so that lower values of $\{\eta, t_{ext}\}$ lead to quantum advantages. For NRM, we consider $g \approx 0$.

with $p_{j,m} = \binom{m}{j} \mu^j (1 - \mu)^{m-j}$ and $\mu = 1 - e^{-\gamma t}$.

We can compute $(\Delta g)_{NRM}^{-2} \equiv \nu \mathcal{F}_C$ using NRM in a similar fashion. For simplicity, we focus on the case $g \approx 0$, which can be solved analytically, but the case of general g can be straightforwardly treated following our previous considerations for TFS. Analogously with our previous considerations, we have,

$$(\Delta g)_{AC}^{-2} = \frac{T}{\sum_{m,l} q(m)q(l)t_{m,l}} \sum_{m,l} q(m)q(l)\mathcal{F}_C^{m,l} \quad (50)$$

with (see Eq. (27)),

$$\mathcal{F}_C^{m,l} = t_{m,l}^2 ((1 - \mu)^{l+1}(l+1)m + (1 - \mu)^{m+1}(m+1)l) \quad (51)$$

with $\mu = 1 - e^{-\gamma t \eta}$.

We show $(\Delta g)_{AC}^{-2}$ in Fig. 8, where it is compared with TFS. In our simulations, we compute $q(k)$ exactly by solving the Hamiltonian Eq. (12) of the main text. As expected, the probabilistic preparation of Fock states in our implementation diminishes its performance with respect to ideal TFS. Yet, we see that already at $n_{ph} \approx 6$, quantum advantages appear possible, even in the presence of detector inefficiencies ($\eta < 1$). The tolerance to imperfections (both η and t_{ext} of $(\Delta g)_{AC}^{-2}$ is shown in Fig. 9.

Implementation of a number resolved measurement in the atomic array

Our previous considerations stress the importance of performing measurements with high reliability ($\eta \approx 1$) and fast ($\gamma t_{ext} \approx 0$), see Fig. 9. Motivated by these constraints, in what follows we develop an implementation of a NRM using the Dicke coupling with the atomic array.

In contrast with the preparation stage, in the initial state the atoms are set in the ground state whereas the photonic state is a Fock state with n_{ph} photons. As in the preparation stage, we can linearize the spin operator (now around the ground state) obtaining $\sum_i \sigma_{\alpha}^- \simeq \sqrt{N_{at}} c_{\alpha}$, where c_{α} is a bosonic annihilation operator. Thus,

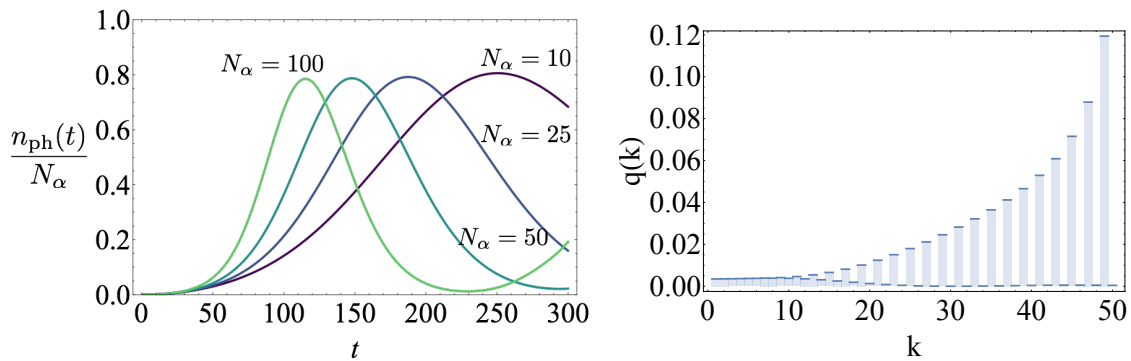


Figure 10. (a) Evolution of the average photon number $n_{\text{ph}}(t)$ in the cavity through the interaction (12). The initial state has N_α excited atoms and cavity in the ground state. The photon number is maximized at a time t^* where $n_{\text{ph}}(t^*)/N_\alpha \approx 0.8$. Parameters: $J = 1$, $\omega_0 = 1$. (b) Probability distribution of the photon number at t^* for $N_\alpha = 50$. Parameters: $J = 1$, $\omega_0 = 1$.

Eq. (12) can now be transformed as

$$H_{\text{Dicke}} \simeq \sum_{\alpha=a,b} \sum_{i=1}^{N_{\text{at}}} [\omega \sigma_{i,\alpha}^z + (J(t) \sqrt{N_{\text{at}}} c_\alpha \alpha^\dagger + \text{H.c.})]. \quad (52)$$

The time evolution is therefore a standard beam splitter interaction with oscillations with period $T = \pi/J\sqrt{N_{\text{at}}}$. We take $t_{\text{meas}} = T/2$, so that all photons are transformed as excitations in the cavity. As discussed in the main text, this has an error probability p_{error} of order $\mathcal{O}((n_{\text{ph}}/N_{\text{at}})^2)$.

Further experimental consideration and implementation in Cavity QED and circuit QED

In practice, there are several additional sources of error in this protocol that ought to be considered.

First, we have assumed that all atoms/qubits are exactly on resonance with the cavity. Realistically, they may have differing energies and be detuned from the cavity, which makes the photon exchange between cavity and atoms less efficient. However, measuring the number of excited atoms after the interaction period still projects the cavity state onto a Fock state, such that disorder only affects the probability distribution of the produced Fock states, but not their fidelity.

Second, the fidelity of the generated Fock state is intrinsically limited by measurement error in the atomic readout. High-fidelity atom readout has already been demonstrated for large numbers of atoms in cavity QED [63–65] and for intermediate numbers of qubits in circuit QED [66–68].

Third, the atoms need to be reset to ground state in a time much faster than $1/g$. This is feasible if the cavity coupling is tunable (e.g., via an intermediate resonator in circuit QED) or if a fast decay channel is used (e.g., a fast optical transition of the atom).

Fourth, no photons may be lost throughout the experiment. This requires ultra-high finesse cavities or long qubit coherence times on the scale of $1/g$, i.e., this requires the strong coupling regime, which has been achieved in both cavity and circuit QED [70–75]. While the measurement is more challenging than the preparation, it relies on the same experimental figures of merit. A large advantage of our scheme is that one can post-select on successful runs of the experiment by requiring that at the end $N_a + N_b$ excitations are measured.

Non-linear regime and optimal time scale

As a final comment, we note that it is in principle possible to use this protocol in the non-linear regime $n_{\text{ph}} = \mathcal{O}(N_{\text{at}})$. Indeed, it might be useful in particular experimental implementations to take most use of the atoms at hand. We hence here discuss a few properties of $q(k)$ and t_{prep} in this regime.

We start by investigating the average photon number $n_{\text{ph}}(t)$ in the cavity during the preparation stage. We see that $n_{\text{ph}}(t)$ reaches its maximum value at $n_{\text{ph}}(t_{\text{opt}}) \approx 0.8N_{\text{at}}$. The distribution $q(k)$ for that optimal time is also illustrated in Fig. 10.

Let us now show that t_{opt} is well approximated by $t_{\text{opt}} \approx \log(4N_{\text{at}})/(2J\sqrt{N_{\text{at}}})$. Let us consider the Hamiltonian

$$H_2 = \frac{1}{2} a^\dagger b^2 + \text{H.c.}, \quad (53)$$

where a, b are the annihilation operators for two harmonic oscillators. a corresponds to what formerly was a spin, and b is just the same cavity mode as before. In the subspace spanned by the states $|N - m\rangle_a \otimes |2m\rangle_b$, where $\{|m\rangle\}$ are Fock states of an oscillator, the Hamiltonian is a bi-diagonal matrix

$$\mathcal{H} = \begin{pmatrix} 0 & a_0 & 0 & \cdots \\ a_0 & 0 & a_1 & \\ 0 & a_1 & 0 & \ddots \\ \vdots & & \ddots & \ddots \end{pmatrix}, \quad (54)$$

where

$$a_m = \sqrt{(N - m)(m + 1/2)(m + 1)} \approx (m + 1)\sqrt{N - m}. \quad (55)$$

For large $N - m$ these are essentially the same matrix elements as the actual Hamiltonian (Eq. (12) in the main text) and one can check numerically that the dynamics is very similar for large enough N . In the classical limit, we replace the annihilation operators by the amplitudes of the corresponding coherent states. The classical (mean field) equations of motion read

$$\frac{d}{dt} \begin{pmatrix} \alpha \\ \beta \end{pmatrix} = -i \begin{pmatrix} \beta^2/2 \\ \beta^* \alpha \end{pmatrix}, \quad (56)$$

with initial conditions $\beta(0) = 1$, $\alpha(0) = \sqrt{N}$.

Now we do a change of variables, taking $\alpha = a \exp(ix)$, $\beta = b \exp(iy)$, such that

$$\dot{a} = -\frac{b^2}{2} \sin \phi, \quad \dot{x} = -\frac{b^2}{2a} \cos \phi, \quad (57a)$$

$$\dot{b} = +ab \sin \phi, \quad \dot{y} = -a \cos \phi, \quad (57b)$$

where $\phi = x - 2y$. Further defining the constant $K = a^2 + b^2/2$, and the variable $r = a^2 - b^2/2$, we obtain the equations of motion

$$\dot{\phi} = -\frac{K + 3r}{\sqrt{2(K + r)}} \cos \phi, \quad (58a)$$

$$\dot{r} = \sqrt{2(K + r)}(K - r) \sin \phi. \quad (58b)$$

This defines a vector field in a two-dimensional plane, whose closed orbits are the possible trajectories of the system. Since the phase ϕ is ill-defined in the initial state, we can choose it to be $\phi = \pi/2$. In this case, the system is governed only by

$$\dot{r} = \sqrt{2(K + r)}(K - r), \quad (59)$$

which is readily integrated to yield

$$\left[\tanh^{-1} \sqrt{\frac{1 + r/K}{2}} \right]_{r(t_i)}^{r(t_f)} = \sqrt{2K}(t_f - t_i). \quad (60)$$

Since initially, $r/K \simeq 1 - 2/N$ and $K \simeq N$ (taking $\alpha = \sqrt{iN}$ and $\beta = 1$), we conclude that the natural timescale for the switch is

$$T \simeq \frac{1}{2\sqrt{N}} \tanh^{-1} \left(1 - \frac{1}{4N} \right) \approx \frac{\log(4N)}{2\sqrt{N}}. \quad (61)$$

This converges to the actual optimal time scale in the limit of large N as we show in Fig. 11.

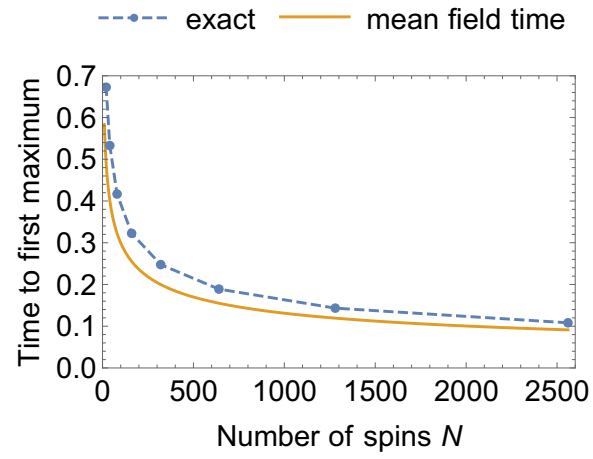


Figure 11. Comparison between the time scale obtained in mean field [Eq. (61)] and the exact timescale calculated numerically.